

Image reconstruction technique and optical monitoring of the QSO2237+0305 from Maidanak Observatory in 2002 – 2003

E. Koptelova^{1*}, E. Shimanovskaya^{1†}, B. Artamonov^{1‡}, M. Sazhin¹, A. Yagola², V. Bruevich¹ and O. Burkhonov³

¹*Sternberg Astronomical Institute, Universitetski pr. 13, 119992 Moscow, Russia*

²*Moscow State University, Faculty of Physics, Vorobiovi Gori, 119992 Moscow, Russia*

³*Ulugh Beg Astronomical Institute of Ac.Sci. of Uzbekistan, Astronomicheskaya 33, 700052 Tashkent, Uzbekistan Republic*

26 August 2004

ABSTRACT

We have observed the gravitational lens system Q2237+0305 from the Maidanak Observatory over the period from August 2002 to November 2003. Here we report the results of our observations. We implemented a two-stage technique that has been developed specifically for the purpose of gravitational lens image reconstruction. The technique is based on the Tikhonov regularization approach and allows one to obtain astrometric and photometric characteristics of the gravitational lens system. Light curves with 78 data points for the four quasar components are obtained. Slow brightness variations over the observational period are found in all components. Images A, C, D have a tendency to decrease in brightness. Image B does not vary more than 0.05mag. The observations did not reveal evidence for large variations in brightness of the components due to microlensing effects. To provide an overall picture of the photometry behaviour, our data are combined with the Maidanak observations published for 1995 – 2000.

Key words: gravitational lensing – galaxies: quasars: individual: Q2237+0305 – techniques: image processing.

1 INTRODUCTION

Since 1997, an international program of gravitational lens monitoring has been carried out at Maidanak Observatory (Uzbekistan) by Tashkent, Moscow and Kharkov observational groups. For the period 1997 – 2003 a huge set of observational data was gathered for the following well known gravitational lens systems: Q2237+0305 (Einstein Cross), SBS1520+530, SBS0909+532, PG1115+080, H1413+117, RX1413+117, RX0921+4528, UM673 (QSO0142-100), B1422+231. The aim of the monitoring program is to obtain light curves for these lens systems.

We have developed a photometric method for the reliable treatment of gravitational lenses with a visible lensing galaxy and applied it to the 2 year dataset of Q2237+0305.

Here, we present results for Q2237+0305, a rather complex system which is the object of monitoring programs of many observational groups. It consists of a barred spiral galaxy at a redshift $z_d=0.039$, in which Huchra et al. (1985) discovered a high-redshift quasar ($z_s=1.695$). The location of the lensed images, which are close to the bulge of the lensing galaxy, makes microlensing events

highly probable in this system (Kayser & Refsdal 1989). The regular observations of Q2237+0305 began from the first microlensing event observed in August 1989 by Irwin et al. (1989). The first attempt to get the light curves of the four quasar components was made by Corrigan et al. (1991). The similar attempt was made in 1994 through constructing light curves which were free from the effects of different spectral bands (Houde M. & Racine S. 1994). The long-duration monitoring program of Q2237+0305 was started in 1990 at the Nordic Optical Telescope (Østensen et al. 1996). During this five-year monitoring program microlensing variations had been detected in all four images. The most densely sampled four-year monitoring was conducted within the OGLE program from August 1997 to November 2000 (Woźniak et al. 2000). It revealed brightness variations in all images and range up to 1.2mag for image C in 1999. The GLITP collaboration presented the results for the period from October 1999 to February 2000 (Alcalde et al. 2002). The GLITP data, which covered a time-period of greater than one month, began after a high magnification microlensing event was observed for the A component by the OGLE collaboration. The monitoring observations from Apache Point Observatory (Schmidt et al. 2002) presented the light curves for only the A and B components of Q2237+0305 from June 1995 to January 1998, but they contained the brightness peak of A component in 1996. The results of VRI photometry in 1997 – 1998 from Maidanak Ob-

* E-mail: koptelova@xray.sai.msu.ru

† E-mail: eshim@sai.msu.ru

‡ E-mail: artamon@sai.msu.ru

servatory were published by Bliokh et al. (1999) and Dudinov et al. (2000). The combined VRI light curves from the monitoring program at the Maidanak Observatory in 1995 – 2000 were presented by Vakulik et al. (2004).

In this paper we present R-band observations of Q2237+0305 from August 2002 to November 2003. The next section describes the conditions of the observations followed by the description of the two-stage image reconstruction technique. We then show the results of the image reconstruction over the observational period and present a photometric variability plot for the quasar components.

2 OBSERVATIONS

Observations of Q2237+0305 were carried out with the 1.5-m AZT-22 telescope of the high-altitude Maidanak Observatory (Uzbekistan) using the LN-cooled CCD camera of Copenhagen University Observatory with the imaging area of 2000×800 and a pixel size of $15 \mu\text{m}$, giving a spatial sampling $0.26 \text{ arcsec pixel}^{-1}$. Data were taken in the Gunn filter, which corresponds approximately to the standard Johnson-Cousins system. The poor tracking available at the telescope only allowed exposures up to a maximum of 3 minutes. To obtain sufficiently high photometric accuracy with such short exposures, the images were taken in series, consisting of 4–8 frames each. The seeing conditions are presented in Tables 3 and 4 via the values of FWHM for particular nights. The best quality of the image corresponds to the point source with $\text{FWHM} = 0.75''$. Pre-processing of the data (including bias-level subtraction, flat-field division, sky subtraction and cosmic ray removal) was done with the standard routines in the Munich Image Data Analysis System (MIDAS) environment. Several stars in the imaging area were used as reference stars to reduce all frames to the same coordinate system. To increase signal-to-noise ratio, and 'to reveal' underlying galaxy several images with excellent seeing ($\text{FWHM} \simeq 0.9''$) were summed before being subjected to photometric processing. Then a subframe of 64 by 64 pixels centred on the nucleus of the galaxy 2237+0305 was extracted.

3 TWO-STAGE IMAGE RECONSTRUCTION ALGORITHM

An essential prerequisite for accurate photometry in ground-based images is good seeing well below the source separation. The extremely compact spatial structure of Q2237+0305, where the component separation is comparable to the seeing, complicates accurate photometry. The presence of the lensing galaxy, with a point-like nucleus and an extended light distribution, makes the photometric results dependant on the galaxy model. This peculiarity leads to poor agreement between the results of different monitoring programs, which adopt different ways to extract the underlying galaxy flux. These difficulties have been noted by many authors (Yee 1988; Corrigan et al. 1991; Vakulik et al. 1997; Burud et al. 1998). In minimization procedures, the galaxy brightness distribution is usually represented either analytically (Østensen et al. 1996; Alcalde et al. 2002; Teuber 1993) or numerically (Burud et al. 1998; Magain et al. 1998). To solve this problem, iterative algorithms are often used to approximately realize minimization of the χ^2 -function. These algorithms estimate the flux contribution from the underlying galaxy, which can then be used in the photometry of the lensed images. Such an approach noticeably simplifies the solution procedure, and provides good intrinsic convergence

(Corrigan et al. 1991; Alcalde et al. 2002; Burud et al. 1998) but unfortunately does not ensure the absence of systematic errors in estimating the magnitudes of the components caused by a poor galaxy model. For the photometry of the data we used a two-stage algorithm developed for the image reconstruction of the objects with point sources superimposed on a smooth background. The algorithm enables the complex images to be split up into the numerical lensing galaxy and quasar components, and allows the galaxy to be subtracted from the individual images which are under consideration. To optimize the photometric treatment of observational data, the process is divided into two stages: 1) combining several images with good seeing and extracting a numerical galaxy model from the combined frame with a regularizing algorithm; 2) processing large numbers of image frames using this numerical galaxy model to get astrometric and photometric characteristics of the gravitational lens system.

The first stage. The first stage of the algorithm is based on the Tikhonov regularization approach. Images obtained on ground-based telescopes affected by the finite instrument resolution and atmospheric perturbations. The simple model of the image formation can be represented as a convolution equation:

$$(t * z)(x, y) = \iint_{\mathbb{B}} t(x - \xi, y - \eta) z(\xi, \eta) d\xi d\eta = u(x, y), \quad (1)$$

where $z(x, y)$ is the unknown light distribution of the object, $u(x, y)$ represents the observable light distribution, the kernel of the above equation $t(x, y)$ is the point spread function (PSF). The estimate of the PSF can be obtained from the images of reference stars in the neighbourhood of the object. In this work two approaches were used to determine the PSF. One approach involves adopting a reference star profile as a numerical point spread function. This method is free of any assumptions about the shape of the PSF, but it depends on the star location because the PSF can vary over the frame field. Another approach involves the theoretical elliptical Gaussian distribution. We also used the semi-analytical RAS (Rotate-And-Stare) method described by Teuber et al. (1994) and employed in the XECClean package by Østensen et al. (1996). PSFs determined with the RAS method are in a good agreement with those theoretically modelled by elliptical Gaussian distributions. The PSF is constructed 1) using an individual star (α) and 2) using the mean brightness distribution obtained via superposition of profiles of reference stars (α, β) weighted inversely proportional to their intensities. The terminology of Yee (1988) and Corrigan et al. (1991) was adopted for the reference stars. We found that the best model for the PSF was obtained using the α star.

The observable data are registered on the pixel grid with some error. The presence of photon noise and, as a consequence, the error of the input data complicates the problem (1) which otherwise can be solved in Fourier space. So, the problem of image reconstruction lies in finding the approximate solution of the equation (1) with the approximate kernel t with known error estimation h :

$$\sup_{\|z\|_Z=1} \|t * z - \bar{t} * z\|_{L_2} \leq h, \quad (2)$$

and having at our disposal the noisy data u and the estimate of the noise level:

$$\sigma_{\text{tot}} : \|u - \bar{u}\|_{L_2} \leq \sigma_{\text{tot}}.$$

Here, barred letters \bar{t} and \bar{u} denote exact, non-error contaminated, PSF and observed image respectively. $\|\cdot\|_Z$ denotes the norm in the Z set of functions. It is assumed that the observed image u belongs to the space L_2 of square integrable functions with the norm:

$$\|u\|_{L_2} \equiv \iint_{\mathbf{B}} u^2(x, y) dx dy \quad (3)$$

The estimation of the σ_{tot} can be calculated as the total noise integrated over the resulting subframe:

$$\sigma_{\text{tot}} = \sqrt{\sum_{i,j} \left(\frac{I_{ij}}{g} + N \cdot R^2 \right)}, \quad (4)$$

where N is the number of summed frames with the same exposure time; I_{ij} – counts in the ij -pixel of the subframe; g – gain factor of the CCD camera; R – readout noise. The error of the operator (2) depends on the method of PSF modeling. If the relative error of PSF modeling is d , then the error of definition of the operator can be estimated as follows:

$$h = \sqrt{\sum_{i,j} (d \cdot t_{ij})^2}. \quad (5)$$

To reduce the systematic errors connected with the galaxy model we try to construct the perfect galaxy model applying regularization techniques. The convolution equation (1) with the error contaminated right-hand side belongs to the class of ill-posed inverse problems. The solution may be non-unique, and small variations in the input data may lead to large variations in the solution. To solve such problems a regularization method was developed by A. Tikhonov (Tikhonov & Arsenin 1977; Tikhonov et al. 1995) that allows to find approximate solution taking into account *a priori* information about the structure of the object. This unique solution, which possesses a specified degree of smoothness and provides a physical representation of the lensing galaxy's flux distribution, tends to the true solution in the norm of the functional space chosen when the errors in input data tend to zero.

The regularization requires construction of an algorithm to control the trade-off between (a) the assumptions about both the smoothness and the structure of the sought solution and (b) its consistency with the data. The key concept of the algorithm is a smoothing function of the following kind:

$$M^\alpha[z] = \|t * z - u\|_{L_2}^2 + \alpha \cdot \Omega[z] \quad (6)$$

Here the first term represents the squared discrepancy between the model and data, α is the regularization parameter which controls the balance between the consistency of the sought solution with the right side of (1) and the smoothness of the sought solution, $\Omega[z]$ is a stabilizer function through which *a priori* information is introduced into the problem formulation (Yagola et al. 2003). Let z^α be the extremum of the function $M^\alpha[z]$ on Z , i.e. z^α is the solution of the minimization problem for $M^\alpha[z]$ on the chosen set of functions (possibly with some constraints).

The choice of the regularization parameter α , which provides uniform residuals and the necessary smoothness of the solution, is crucial for solving ill-posed problems. Generally, it should depend on the input data, the errors, and the method of approximation of the initial problem. One of the way to co-ordinate the regularization parameter with the error of the input information is the discrepancy principle – adoption of $\alpha > 0$ satisfying:

$$\|t * z^\alpha - u\|_{L_2} \simeq \sigma_{\text{tot}}. \quad (7)$$

The regularization parameter α is chosen such that the corresponding residual (the left hand side of (7)) is equal to the a priori specified bound (right hand side) for the noise level in the image. The regularization method with α chosen according to the discrepancy principle (7) is convergent and of optimal order (Morozov 1984;

Engl 2000). Provided that the regularization parameter α is chosen according to this rule, the solution z^α of the minimization problem for $M^\alpha[z]$ can be considered as an approximate solution. The approximate solution obtained using this method goes to the true solution when the error of input data goes to zero.

When the kernel t in (1) is known inexactly, one can use the generalized discrepancy principle (Tikhonov et al. 1998) which lies in solving the following equation:

$$\rho(\alpha) = 0 \quad (8)$$

where $\rho(\alpha)$ is called the generalized discrepancy:

$$\rho(\alpha) \equiv \|t * z^\alpha - u\|_{L_2}^2 - \left(\sigma_{\text{tot}} + h \sqrt{\Omega[z^\alpha]} \right)^2. \quad (9)$$

The function $\rho(\alpha)$ is strictly monotonic and the root of (8) can be found by bisection or some other standard method. This is an *a posteriori* method of choosing the regularization parameter, because, to find the root of equation (8), one needs to minimize the smoothing function at every iteration by α . Given the estimations of σ_{tot} and h we used the generalized discrepancy principle to choose the regularization parameter.

Various assumptions about the structure of the object under study can also be taken into account. Images of close quadruple gravitational lens systems consist of multiple overlapped quasar images superimposed on a lensing galaxy. So, the image can be decomposed into two constituent parts: the sum of four δ -functions and smooth background (galaxy). Written for the pixel grid, that assumption is represented as follows:

$$z_{mn} = \sum_{q=1}^4 a_q \delta_{m-b_q, n-c_q} + g_{mn}, \quad (10)$$

where a_q are the intensities of point sources with coordinates (b_q, c_q) , $\delta_{m-b_q, n-c_q}$ are Kronecker deltas, g_{mn} is the solution's component corresponding to the lensing galaxy.

Numerical simulations revealed that introducing the assumption about the closeness of the real galaxy light distribution to some analytical profile produces more stable results for the reconstruction. In this work we assume that the light distribution in the central region of the galaxy is well-modelled by a generalized de Vaucouleurs profile (De Vaucouleurs 1948, 1959), known as Sersic's model (Sersic 1968; Cardone 2004):

$$g^{\text{mod}}(r) = I_e \exp \left(-b_n \left(\frac{r}{r_e} \right)^{\frac{1}{n}} \right), \quad (11)$$

where $b_n = 2n - 0.324$ for $1 < n < 4$ ($n = 4$ corresponds to de Vaucouleurs model), r_e is an effective radius, I_e is an intensity within the effective radius, and $r(x_c, y_c, a_x, a_y, \theta)$:

$$r^2 = \frac{x'^2}{a_x^2} + \frac{y'^2}{a_y^2} \quad (12)$$

where x' and y' are measured from the centre along the major and minor axes.

Given the image, one can represent it in accordance with (10) where the lensing galaxy is described with the analytical model (11). Parameters of the analytical model are fitted by means of minimization of the χ^2 -function:

$$\begin{aligned} \chi^2(a_q, b_q, c_q, I_e, r_e, n, x_c, y_c, a_x, a_y, \theta) = \\ = \sum_{i,j} \frac{N_1 N_2}{\sigma_{ij}^2} \left(\sum_{m,n} t_{i-m, j-n} \cdot z_{mn}^{\text{mod}} - u_{ij} \right)^2, \end{aligned} \quad (13)$$

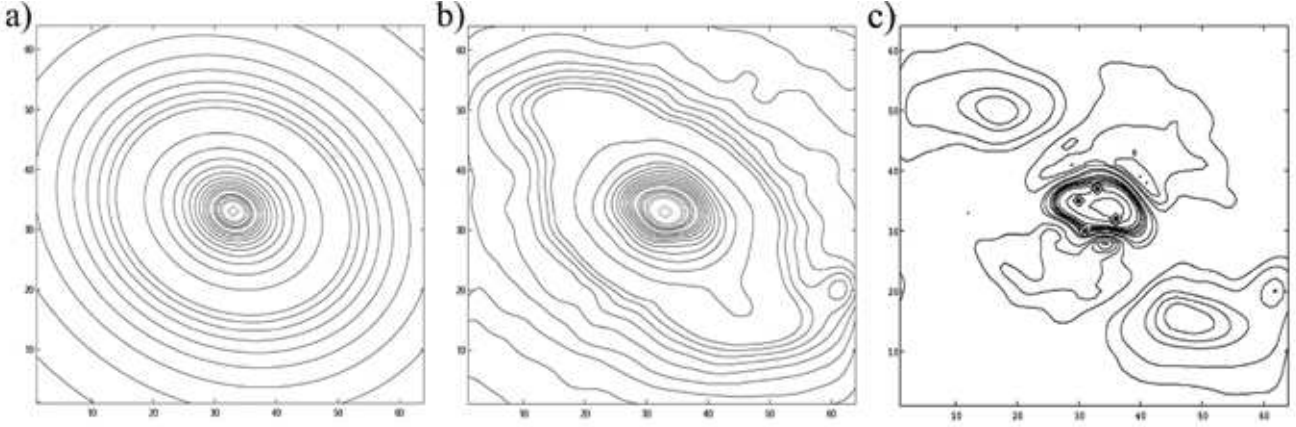


Figure 1. The contours of the central region ($17.14'' \times 17.14''$) of the lensing galaxy: a) the analytical galaxy model (Sersic model fitting); b) the numerical galaxy model (Tikhonov regularization algorithm); c) the difference between a) and b) with the quasar components superimposed.

$$z_{mn}^{\text{mod}} = \sum_{q=1}^4 a_q \delta_{m-b_q, n-c_q} + g_{mn}^{\text{mod}},$$

where σ_{ij} is the noise in each pixel of the frame. The positions of quasar components (b_q, c_q), the corresponding amplitudes a_q , and the analytical galaxy model parameters are fitted. Powell (Press et al. 1998) method is used as a minimization routine.

Given the assumption that the real galaxy light distribution is close to the analytical profile the stabilizer function in (6) can be written as follows:

$$\Omega[z] = \|g^{\text{num}} - g^{\text{mod}}\|_G^2 + \beta \sum_{q=1}^4 a_q^2, \quad (14)$$

where g^{num} is a sought numerical galaxy model, g^{mod} is the analytical galaxy model. The second term in the right-hand side is introduced in order to penalize values of quasar intensities that are too large compared to the lensing galaxy. The parameter β is chosen on the basis of the model calculations in the way that both terms in the stabilizer function are of the same order. Such an approach enables probable artefacts in the galaxy brightness distribution ('holes' at the positions of quasar components) to be excluded.

After the parameters of the analytical galaxy model g^{mod} have been found, this model is used for construction of the stabilizer function and as an initial approach for minimization of the smoothing function:

$$M^\alpha(a_q, g^{\text{num}}) = \sum_{i,j} \frac{1}{\sigma_{ij}^2} \left(\sum_{m,n} t_{i-m, j-n} z_{mn} - u_{ij} \right)^2 + \alpha \sum_{i,j} (g_{ij}^{\text{num}} - g_{ij}^{\text{mod}})^2 + \beta \sum_{q=1}^4 a_q, \quad (15)$$

$$z_{mn} = \sum_{q=1}^4 a_q \delta_{m-\bar{b}_q, n-\bar{c}_q} + g_{mn}^{\text{num}}.$$

Here (\bar{b}_q, \bar{c}_q) are the fixed quasar components coordinates from the preliminary step. The method of conjugate gradients was used to construct the minimizing sequence (Press et al. 1998).

Due to the huge number of free parameters the process of minimizing the smoothing function is time-consuming. The main result at this stage is the numerical galaxy model. After the accurate nu-

Table 1. Parameters of the lensing galaxy: r_e – effective radius, ϵ – ellipticity, P.A. – position angle.

images	r_e ($''$)	ϵ	P.A. ($^\circ$)
H CASTLES	4.7 ± 0.9	0.33 ± 0.01	66 ± 1
R GLITP	4.94 ± 0.25	0.38 ± 0.02	62 ± 1
R Maidanak	4.6 ± 0.3	0.35 ± 0.02	64 ± 1

merical galaxy model is found, the huge data set for the same observational period can be processed in a much shorter space of time. The equal brightness contours for the central part of the galaxy for both analytical and numerical galaxy models are presented in Fig. 1. The mean values of the galaxy parameters from the CASTLE collaboration in H filter, the GLITP collaboration, and our values derived from the first stage of the two-stage image reconstruction algorithm in R filter are combined in Table 1.

The second stage. In the second stage, the numerical galaxy model g^{num} , obtained in the previous stage as a result of the minimization of the Tikhonov regularization function (15), is used for the photometric treatment of all observational data. For every individual frame the galaxy brightness distribution is described as follows:

$$G_{mn} = \lambda_1 \cdot g_{mn}^{\text{num}} + \lambda_2, \quad (16)$$

where λ_1 is a multiplier giving a level of the galaxy intensity in every individual frame, λ_2 is some additional constant background. So, since a galaxy in the second stage is described only by two parameters, the number of parameters are reduced allowing a decrease in processing time. The finite-dimensional solution of this fitting problem can be found by minimizing a χ^2 -function of the following form:

$$\chi^2(a_q, b_q, c_q, \lambda_1, \lambda_2) = \sum_{i,j} \frac{1}{\sigma_{ij}^2} \left(\sum_{m,n} \{t_{i-m, j-n} (\sum_{q=1}^4 a_q \delta_{m-b_q, n-c_q} + G_{mn})\} - u_{ij} \right)^2.$$

As far as exposure time for all processed frames is the same, the overall brightness of the galaxy in the subframe should be nearly constant. Calculations exhibited that the parameter λ_1 fluctuates by 1.4% from subframe to subframe. That slight variation might be due to different seeing conditions.

The results of the image reconstruction from the second stage are presented in Fig. 2.

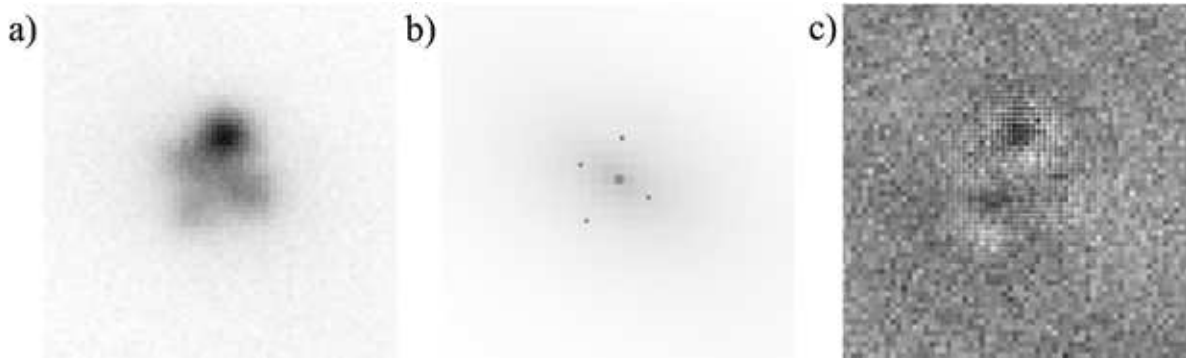


Figure 2. Results of the image reconstruction of gravitational lens system Q2237+0305 (Einstein Cross) with our two-stage algorithm: a) observed image (*OBS*); b) reconstructed image (*REC*); c) residuals ($\frac{OBS - convolved REC}{\sqrt{convolved REC}}$)

Table 2. Astrometry of the components of Q2237+0305 relative to A component.

	H CASTLES		R Maidanak	
	$\Delta R.A. (")$	$\Delta Dec. (")$	$\Delta R.A. (")$	$\Delta Dec. (")$
B	-0.673 ± 0.003	1.697 ± 0.003	-0.723 ± 0.052	1.646 ± 0.058
C	0.635 ± 0.003	1.209 ± 0.003	0.567 ± 0.069	1.211 ± 0.016
D	-0.866 ± 0.003	0.528 ± 0.003	-0.858 ± 0.016	0.534 ± 0.016
G	-0.075 ± 0.003	0.939 ± 0.003	-0.094 ± 0.028	0.937 ± 0.027

4 RESULTS

We have developed a two-stage technique for the image reconstruction of objects with a complex structure that consist of point sources superimposed on a smooth lensing galaxy. The algorithm that we have developed has been shown to perform well in reconstructing images of a quadruple gravitational lens system. We believe it is flexible enough to be applied to other objects with structure of a similar complexity. The algorithm allows the adoption of different analytical models to 'adjust' a numerical galaxy model and also allows the choice of different sets of functions to control the smoothness of the background constituent (lensing galaxy) of the solution.

The technique was used to process the two-year observational data for the close quadruple gravitational lens system Q2237+0305, well known for its complex structure and the small separation between quasar components. The correct photometry for such kind of objects is not possible without constructing as realistic a model for the underlying galaxy as possible. We try to get an accurate galaxy model by avoiding an analytical description of the galaxy. This ensures that the numerical galaxy model obtained in the first stage of the algorithm is free from any disadvantages associated with an analytical model. Fig. 1 shows contours of analytical (a) and numerical (b) galaxy models constructed in the first stage of the algorithm. The contour map of the difference between the analytical and numerical galaxy models in the Fig. 1c) reveals an uncertainty in the central region where the quasar components are located, and in the spiral barred regions. Fig. 1b) shows that the numerical galaxy has a realistic structure with arms. It is evident that the residual map in Fig. 2c) does not contain any significant contribution from the spiral arms of the galaxy, unlike the analytical galaxy modelling approach. The numbers of quasar image positions are presented in the Table 2 along with CASTLES data.

To evaluate the ability of the algorithm to fit the observational

data, the χ^2 per degree of freedom ($\bar{\chi}^2$) was used. In this problem the number of degrees of freedom is equal 4108, corresponding to the pixel size of the frame which is under the treatment (64×64 pixels) plus two coordinates and the flux of each quasar component. The reduced $\bar{\chi}^2$ value for the two-stage image reconstruction method varied in the range of 1.2 to 9.0.

The compactness of the system (approximately 2 arcsec) further complicates the photometric treatment. Unfortunately, despite the intrinsically good seeing, a poor telescope tracking system significantly reduces the quality of the data and in some cases induces ellipticity in the PSF. In our data processing we use two strategies for the PSF construction. In cases where the image quality was compromised by the poor tracking system, the numerical PSF seems to be more suitable.

We present monitoring data of Q2237+0305 over the period from 28 August 2002 to 27 November 2003. The R-band light curves for the four images are shown in Fig. 3 and tabulated in Tables 3 and 4. Since Maidanak data have been taken in Gunn r-band, the reference α star with known r-magnitude determined by Corrigan et al. (1991) was used for the calibration of the Q2237+0305 data. Transition to the standard system was carried out according to the color equation with coefficients derived from the Maidanak observations of the Landolt standards fields (Landolt A. 1992). The color correction was done using the results from Vakulik et al. (2003). The quoted error values in Tables 3 and 4 are the standard deviation of the processed frames for one night. Note that these errors do not include any error associated with the method, since this is impossible to calculate for ill-posed problems.

5 DISCUSSION

In Fig. 4 we have combined the R-band light curves for the four quasar components of Q2237+0305 over the period from 1995 to 2003, based on data obtained in 1995 – 2000 by Vakulik et al. (2003) and on the results of the photometry treatment for 2002 – 2003 presented in this paper. All plotted data correspond to observations conducted at the Maidanak Observatory.

As can be seen, trends in the light curves of the C and D components are fairly similar. The other two components show less agreement. There is a drop for the A component in the July 2003 data points, but there is a rise of 0.2mag at the end of the light curve. Future behaviour of this component could be detected with further

observations. For the B component the light curve is flatter than for the others. As the B component of the system is the faintest one, some discrepancies for several days and the large scatter in the data points may be due to days with bad seeing.

It is useful to compare the presented results with ones obtained for the same observational period with another photometry method. To test our two-stage image reconstruction algorithm, we processed several images from the Maidanak dataset with the CLEAN procedure (Østensen et al. 1996) which revealed that for the images with seeing 0.8-0.9 arcsec the results of the photometry for the A component match those obtained using the proposed technique. Getting accurate quasar image positions, which maximize the correlation coefficients of the CLEAN method, from images with worse seeing is rather problematic, considering that correlation coefficients less than 0.98 lead to unacceptable large uncertainty in the magnitude values.

Another test for the algorithm is the comparison of the results with light curves obtained by OGLE monitoring program (<http://www.astrouw.edu.pl/~ogle/ogle3/huchra.html>). Fig. 3 shows a good agreement between the results of two-stage algorithm and photometry of Q2237+0305 in V band by OGLE program.

ACKNOWLEDGMENTS

The authors would like to thank the referee for a very helpful report.

We gratefully acknowledge the use of data obtained by the German-Uzbek collaboration between Potsdam University (Robert Schmidt, Joachim Wambsganss), Astrophysical Institute Potsdam (Stefan Gottlöber, Lutz Wisotzki) and the Ulugh Beg Astronomical Institute Tashkent (Salakhutdin Nuritdinov).

This research was supported by Russian Foundation for Basic Research (RFBR) grants 02-01-00044, and 01-02-16800. We thank Alexandr Gusev for providing transformation coefficients of the Maidanak instrumental system to the standard photometric system, and Vasily Belokurov for detail discussion of this work and helpful suggestions. We thank Andrzej Udalski for the attention to our work, and Martin Smith for the careful reading of the paper.

REFERENCES

- Alcalde D., Mediavilla E., Moreau O., et al. 2002, *ApJ*, 572, 729A
- Bliokh P.V., Dudinov V.N., Vakulik V.G., et al. 1999, *Kin.&Phys.Cel.Bodies*, 15, 338
- Burud I., Stabell R., Magain P., et al., 1998, *A&A*, 339, 701
- Cardone V.F., 2004, *A&A*, 415, 3
- Corrigan R.T., Irwin M.J., Arnaud J., et al., 1991, *Astron. J.*, 102, 34
- De Vaucouleurs G., 1948, *Ann. Astrophys.*, 11
- De Vaucouleurs G., 1959, *Hand. Phys*, 53
- Dudinov V.N., Vakulik V.G., Zheleznyak A.P., et al. 2000, *Kin.&Phys.Cel.Bodies*, 16, 346
- Engl H. W., Hanke M. and Neubauer A., 2000, *Regularization of inverse problems*, Kluwer Academic Publishers
- Houde M., and Racine R., 1994, *AJ*, 107, 466
- Huchra J. et al., 1985, *AJ*, 90, 691
- Irwin M.J. et al., 1989, *Nature* 338, 6218, 745
- Kayser R., Refsdal S., 1989, *AJ*, 98, 1989
- Landolt A.U., 1992, *AJ.*, 104, 340
- Magain P., Courbin F. and Sohy S., 1998, *ApJ*, 494, 472
- Morozov V.A., 1984, *Methods for solving incorrectly posed problems*, Springer-Verlag New York Inc.
- Østensen R., Refsdal S., Stabell R., et al. 1996, *A&A*, 309, 59
- Press W.H., Teukolsky S.A., Vetterling W.T., and Flannery B.P. *Numerical Recipes in C*, Camb. Univ. Press, 1998
- Schmidt R. W., Kundic N., Pen U.-L., et al. 2002, *A&A*, 392, 773
- Sersic J. L. 1968, *Atlas de Galaxias Australes*, Observatorio Astronomico, Cordoba, Argentina
- Teuber J., 1993, *Digital Image Processing*, Prentice-Hall
- Teuber J., Østensen R., Stabell R., and Florentin-Nielsen R., 1994, *Ap&A, Suppl. ser.*, 108, 509
- Tikhonov A.N., Arsenin V.Y., 1977, *Solutions of Ill-posed Problem*, Wiley, New York.
- Tikhonov A.N., Goncharky A.V., Stepanov V.V. and Yagola A.G., 1995, *Numerical methods for the solution of ill-posed problems*, Kluwer Academic Press, Dordrecht.
- Tikhonov A.N., Leonov A.S., Yagola A.G., 1998, *Nonlinear ill-posed problems*, V.1, Chapman and Hall, London.
- Vakulik V.G., Dudinov V.N., Zheleznyak A.P., Tsvetkova V.S., 1997, *Astron. Nachr.*, 318, 73
- Vakulik V.G. et al., *astro-ph/0312631*
- Vakulik V.G., Schild R.E., Dudinov V.N., et al. 2004, *A&A* (accepted 13/02/2004)
- Woźniak P.R., Alard C., Udalski A., et al. 2000, *ApJ*, 529, 88
- Yagola A., Artamonov B., Belokurov V., Koptelova E., Shimanovskaya E., 2003, *Inverse Problems in Engineering Mechanics IV: international symposium on inverse problems in engineering mechanics (ISIP 2003)*, Masataka Tanaka (Ed.), Elsevier
- Yee H.K.C., 1988, *Astron. J.*, 95, 1331

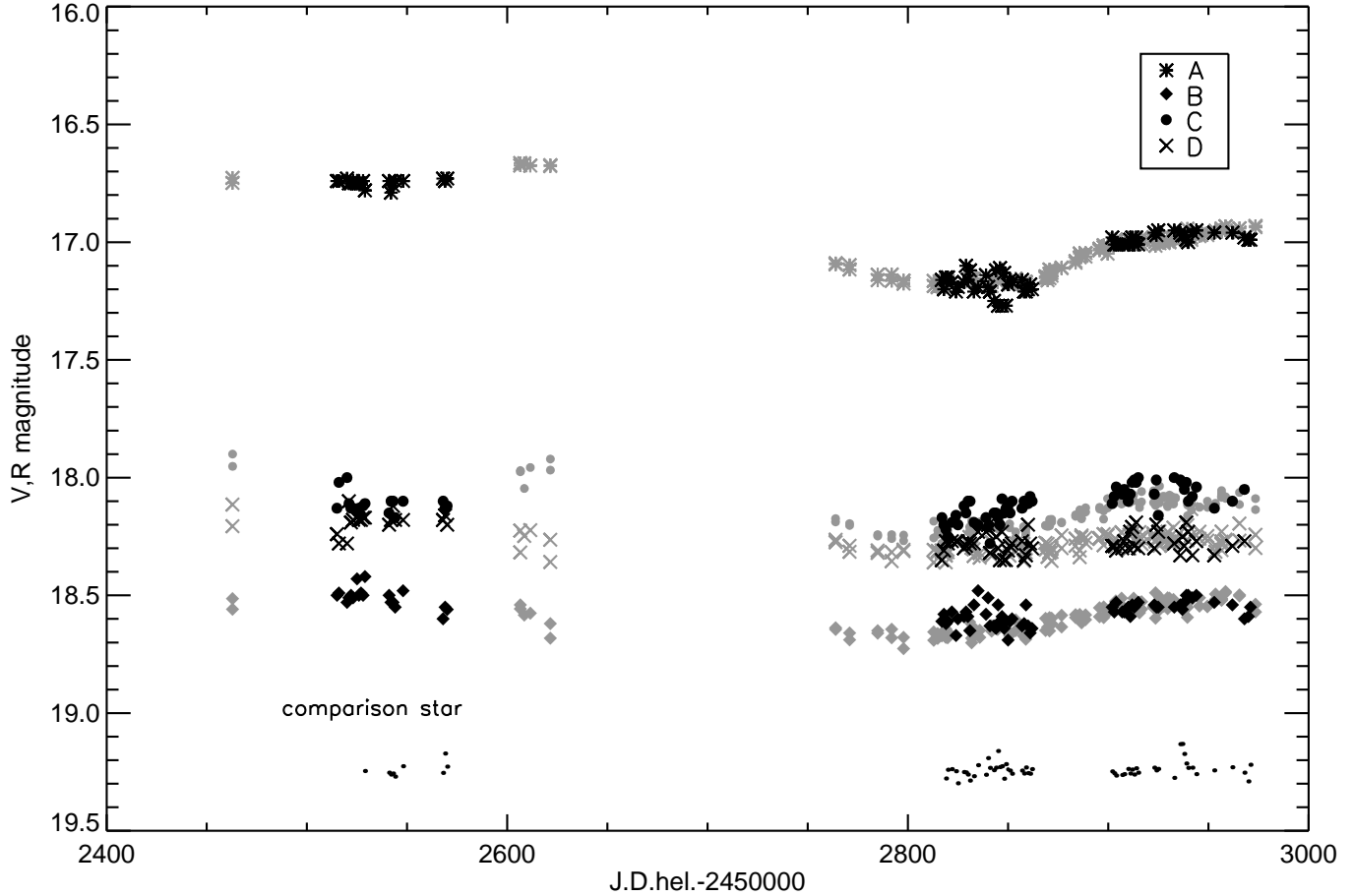


Figure 3. Photometry of Q2237+0305 in R band from observations with 1.5-m Maidanak telescope in 2002-2003. Photometry in V band by OGLE program (<http://www.astrouw.edu.pl/~ogle/ogle3/huchra.html>) is also plotted by fainter symbols. The comparison star (α) is shifted in magnitude by 2.7mag.

Table 3. Photometry of Q2237+0305 in R filter from observations at Maidanak Observatory in 2002. The table contains the date in yymmdd format, the Julian date (-2450000), the seeing as determined from α star and the magnitudes of four quasar components.

date	Julian date	seeing (arcsec)	A	B	C	D
02.08.28	2515	0.8	16.74±0.01	18.62±0.02	18.21±0.01	18.23±0.02
02.08.29	2516	0.9	16.74±0.04	18.49±0.04	18.02±0.04	18.38±0.06
02.09.02	2520	1.3	16.73±0.03	18.53±0.07	18.00±0.09	18.28±0.09
02.09.03	2521	1.2	16.75±0.01	18.51±0.05	18.11±0.07	18.10±0.09
02.09.04	2522	0.8	16.75±0.01	18.50±0.10	18.13±0.03	18.19±0.03
02.09.05	2523	0.7	16.74±0.02	18.51±0.09	18.13±0.02	18.18±0.09
02.09.07	2525	0.8	16.75±0.07	18.43±0.02	18.14±0.03	18.17±0.05
02.09.08	2526	0.9	16.75±0.02	18.50±0.02	18.13±0.05	18.18±0.05
02.09.09	2527	0.8	16.75±0.03	18.49±0.07	18.16±0.09	18.18±0.04
02.09.10	2528	0.8	16.74±0.01	18.50±0.02	18.12±0.03	18.17±0.02
02.09.17	2529	1.1	16.78±0.07	18.42±0.10	18.11±0.03	18.10±0.10
02.09.23	2541	1.1	16.74±0.07	18.50±0.08	18.15±0.05	18.10±0.20
02.09.24	2542	1.0	16.79±0.05	18.53±0.09	18.10±0.04	18.18±0.01
02.09.25	2543	1.0	16.76±0.03	18.53±0.05	18.15±0.04	18.12±0.09
02.09.26	2544	1.3	16.74±0.07	18.64±0.19	18.17±0.13	18.16±0.09
02.09.30	2548	1.0	16.74±0.05	18.48±0.10	18.10±0.12	18.18±0.09
02.10.20	2568	0.9	16.73±0.04	18.60±0.10	18.10±0.05	18.18±0.07
02.10.21	2569	1.0	16.74±0.02	18.55±0.08	18.13±0.09	18.16±0.03
02.10.22	2570	0.9	16.73±0.03	18.56±0.07	18.12±0.07	18.20±0.05

Table 4. Photometry of Q2237+0305 in R filter from observations at Maidanak Observatory in 2003. The table contains the date in yymmdd format, the Julian date (-2450000), the seeing as determined from α star and the magnitudes of four quasar components.

date	Julian date	seeing (arcsec)	A	B	C	D
03.06.26	2817	1.3	17.16±0.06	18.61±0.10	18.21±0.11	18.35±0.08
03.06.27	2818	1.0	17.20±0.09	18.58±0.10	18.18±0.08	18.32±0.11
03.06.28	2819	1.1	17.15±0.04	18.62±0.09	18.17±0.11	18.35±0.17
03.06.29	2820	0.9	17.15±0.05	18.61±0.09	18.20±0.07	18.31±0.11
03.07.01	2822	1.0	17.17±0.07	18.57±0.01	18.22±0.09	18.27±0.11
03.07.03	2824	1.7	17.21±0.12	18.67±0.11	18.25±0.15	18.28±0.15
03.07.04	2825	1.0	17.19±0.07	18.60±0.10	18.19±0.04	18.27±0.13
03.07.07	2828	0.9	17.17±0.04	18.59±0.09	18.16±0.07	18.27±0.10
03.07.08	2829	1.0	17.10±0.02	18.57±0.08	18.20±0.13	18.27±0.09
03.07.09	2830	1.5	17.16±0.07	18.59±0.10	18.12±0.11	18.30±0.12
03.07.10	2831	1.5	17.12±0.05	18.65±0.12	18.15±0.11	18.29±0.13
03.07.12	2833	1.4	17.21±0.07	18.54±0.09	18.10±0.08	18.27±0.11
03.07.14	2835	1.1	17.19±0.06	18.48±0.12	18.10±0.06	18.28±0.08
03.07.18	2839	1.2	17.14±0.09	18.58±0.09	18.19±0.11	18.28±0.12
03.07.19	2840	1.0	17.19±0.06	18.51±0.09	18.20±0.09	18.23±0.11
03.07.20	2841	1.2	17.21±0.03	18.63±0.04	18.17±0.09	18.23±0.03
03.07.22	2843	1.4	17.25±0.07	18.63±0.10	18.21±0.11	18.20±0.07
03.07.23	2844	1.3	17.12±0.09	18.64±0.10	18.28±0.11	18.32±0.21
03.07.24	2845	1.3	17.27±0.09	18.54±0.09	18.15±0.05	18.20±0.18
03.07.25	2846	1.2	17.11±0.06	18.61±0.10	18.15±0.09	18.25±0.08
03.07.26	2847	1.1	17.27±0.09	18.59±0.09	18.17±0.05	18.30±0.11
03.07.27	2848	1.4	17.13±0.09	18.64±0.09	18.20±0.08	18.35±0.18
03.07.28	2849	1.2	17.27±0.09	18.61±0.06	18.09±0.06	18.23±0.10
03.07.29	2850	1.2	17.18±0.07	18.69±0.09	18.15±0.04	18.35±0.15
03.07.30	2851	1.2	17.16±0.08	18.61±0.09	18.13±0.10	18.35±0.14
03.07.31	2852	0.9	17.17±0.04	18.60±0.09	18.12±0.07	18.31±0.13
03.08.05	2857	1.2	17.16±0.09	18.63±0.10	18.15±0.07	18.29±0.07
03.08.06	2858	0.9	17.21±0.05	18.62±0.09	18.10±0.07	18.28±0.10
03.08.07	2859	0.9	17.21±0.08	18.54±0.03	18.13±0.06	18.27±0.17
03.08.08	2860	0.9	17.20±0.04	18.63±0.10	18.10±0.08	18.35±0.11
03.08.09	2861	0.8	17.18±0.04	18.66±0.09	18.11±0.08	18.33±0.08
03.08.10	2862	0.9	17.20±0.03	18.64±0.09	18.11±0.04	18.20±0.17
03.09.19	2902	1.1	16.98±0.07	18.55±0.07	18.07±0.11	18.28±0.12
03.09.20	2903	0.8	17.01±0.05	18.57±0.08	18.10±0.09	18.30±0.04
03.09.21	2904	1.3	17.01±0.08	18.53±0.08	18.11±0.11	18.29±0.18
03.09.24	2907	1.1	17.01±0.03	18.57±0.07	18.08±0.09	18.29±0.09
03.09.25	2908	1.0	17.01±0.04	18.57±0.07	18.04±0.05	18.31±0.11
03.09.27	2910	1.3	17.01±0.04	18.55±0.09	18.07±0.05	18.30±0.13
03.09.28	2911	1.4	16.99±0.09	18.59±0.11	18.05±0.11	18.27±0.19
03.09.29	2912	1.2	16.98±0.09	18.54±0.09	18.10±0.10	18.30±0.15
03.09.30	2913	0.8	17.01±0.03	18.55±0.08	18.07±0.06	18.23±0.08
03.10.01	2914	0.9	16.98±0.06	18.54±0.07	18.02±0.04	18.21±0.13
03.10.02	2915	0.8	17.01±0.05	18.53±0.07	18.01±0.09	18.29±0.07
03.10.10	2923	0.9	16.96±0.02	18.54±0.02	18.02±0.07	18.19±0.09
03.10.11	2924	1.0	16.97±0.02	18.55±0.03	18.00±0.07	18.30±0.10
03.10.12	2925	1.1	16.95±0.02	18.55±0.05	18.07±0.08	18.30±0.18
03.10.20	2933	1.0	16.95±0.02	18.55±0.05	18.01±0.03	18.20±0.12
03.10.23	2936	1.4	16.96±0.03	18.54±0.06	18.16±0.04	18.23±0.15
03.10.24	2937	1.1	16.97±0.03	18.56±0.04	18.00±0.07	18.28±0.09
03.10.25	2938	0.9	16.97±0.03	18.53±0.07	18.01±0.07	18.33±0.13
03.10.26	2939	1.1	16.99±0.05	18.50±0.06	18.02±0.06	18.25±0.05
03.10.27	2940	1.4	17.00±0.05	18.50±0.07	18.05±0.09	18.29±0.11
03.10.29	2942	1.0	16.96±0.05	18.51±0.03	18.02±0.08	18.19±0.13
03.10.31	2944	1.2	16.95±0.03	18.50±0.03	18.10±0.08	18.23±0.18
03.11.09	2953	1.2	16.96±0.02	18.53±0.06	18.08±0.06	18.33±0.14
03.11.18	2962	0.9	16.96±0.02	18.54±0.05	18.04±0.03	18.27±0.09
03.11.24	2968	1.1	16.98±0.05	18.60±0.08	18.13±0.05	18.33±0.11
03.11.26	2970	1.4	16.99±0.10	18.59±0.10	18.10±0.08	18.29±0.20
03.11.27	2971	0.9	16.99±0.04	18.55±0.05	18.05±0.07	18.27±0.09

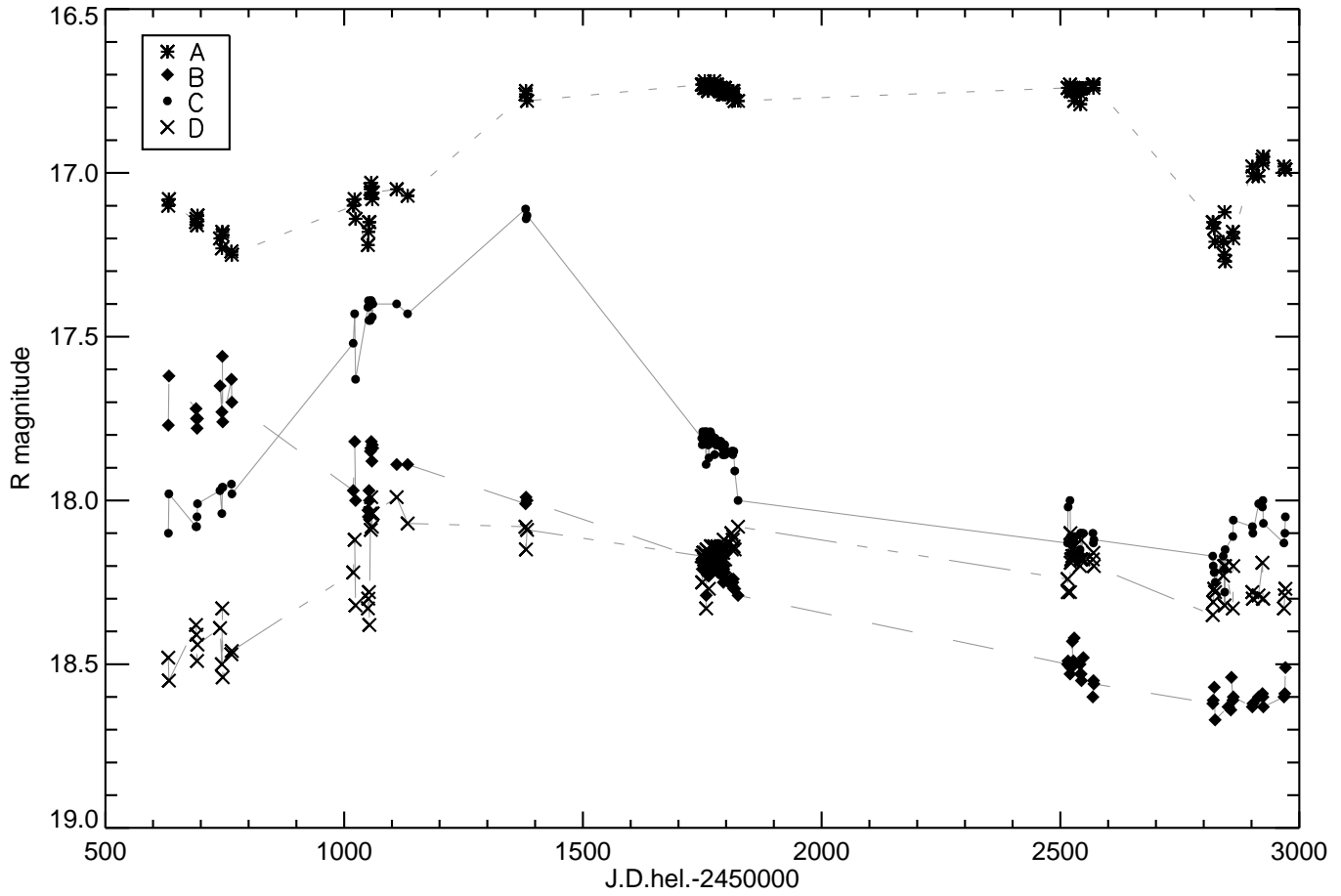


Figure 4. Combined Q2237+0305 light curves in the R band for 1995 – 2003 based on data from Vakulik et al. (2003) and from this paper.